



Improving the quality of gluten-free plant-based meat analogs based on soy protein isolate with insoluble soy fibers and low acyl gellan gum

Somayeh Taghian Dinani^{1,2} · Stijn de Jong¹ · Bongkosh Vardhanabhuti² · Atze Jan van der Goot¹

Received: 8 July 2023 / Revised: 2 October 2023 / Accepted: 13 October 2023
© The Author(s) 2023

Abstract

This study describes the effects of incorporating insoluble soy fiber and low acyl gellan gum as an alternative for wheat gluten in plant-based meat analogs made from soy protein isolate (SPI). The formulations containing insoluble soy fiber (ranging from 0 to 3%) and low acyl gellan gum (0–2%) were processed in a high-temperature shear cell (HTSC) and then analyzed in terms of macrostructure, microstructure, rheological properties, tensile strength, and water absorption capacity (WAC). Macrostructural analysis revealed that the control product containing SPI without insoluble soy fiber and low acyl gellan gum exhibited a dense and gel-like structure, devoid of visible fibers. The addition of 1, 2, and 3 wt.% of insoluble soy fiber increased the formation of visually elongated fibers in both macro- and microscopic levels in the shear direction, resulting in anisotropic plant-based meat analogs with improved tensile strength and elasticity. The use of 1 and 2 wt.% low acyl gellan gum led to the formation of short and thin filaments that were less oriented in the shear direction, resulting in decreased tensile strength. When combined with low acyl gellan gum, insoluble soy fiber failed to produce lengthy and elongated fibers, resulting in short and thin fibrils. These findings suggest that the interaction between insoluble soy fiber and low acyl gellan gum under the processing conditions may hinder fiber formation and mechanical anisotropy. Microscopic examination reveals smoother regions in products enriched with insoluble soy fiber and rougher surfaces in those containing low acyl gellan gum. Moreover, X-ray microtomography confirms that insoluble soy fiber enhanced air retention, contributing to enhanced structural integrity. In contrast, low acyl gellan gum introduces irregularly shaped air bubbles, compromising structural improvement. In summary, this study underscores the potential of insoluble soy fiber to enhance the structural and the textural properties of plant-based meat analogs. However, it also highlights the challenges posed by low acyl gellan gum, which, despite improving water retention, may hinder fiber formation and mechanical anisotropy. These findings offer insights for advancing the quality of plant-based meat products.

Keywords Insoluble soy fiber · Low acyl gellan gum · Shear-induced deformation · Macro- and microstructural properties · Meat analogs

Introduction

The global human population has surpassed 8 billion and continues to grow [27], creating a pressing challenge, which is to ensure an adequate food supply, especially protein, for this expanding population. Among other due to the growing population, the meat industry is expected to grow by 7.5% annually to meet the demand [20]. This growth carries negative environmental and ethical consequences, sparking a call for change [11]. A potential solution lies in the development of plant-based meat analogs, where food technologists play a pivotal role in improving their texture and developing new formulations [12]. Meat analogs can offer an alternative

✉ Somayeh Taghian Dinani
somayeh.taghiandinani@wur.nl; stvm3@umsystem.edu

✉ Atze Jan van der Goot
atzejan.vandergoot@wur.nl

¹ Food Process Engineering, Wageningen University and Research, PO Box 17, 6700 AA Wageningen, The Netherlands

² Division of Food, Nutrition, and Exercise Sciences, University of Missouri, Columbia, MO 65211, USA

protein source to address the protein needs without relying on traditional meat sources.

This study employs high-temperature shear cell (HTSC) technology to create plant-based meat analogs that mimic meat-like structures using plant proteins in doughs, while employing milder processing conditions compared to commercially used extruders [9]. The dough's composition significantly affects the outcome, with properties influenced by interactions among proteins, fibers, and hydrocolloids being present in continuous and dispersed phases during and after processing. Current formulations of plant-based meat analogs often contain wheat gluten (WG) alongside soy protein concentrate (SPC) or soy protein isolate (SPI). However, the presence of WG poses issues for those with celiac disease [26]. Yet, the elimination of WG from the formulation of plant-based meat analogs can hinder fiber formation during processing. One possible approach to address this dilemma involves substituting WG with insoluble fibers and hydrocolloids, and combinations thereof.

Plant fibers, comprising cellulose, hemicellulose, pectin, glycoproteins, and lignin, are essential compounds of plant cell walls, providing structural support. While SPC contains 10–20% fiber, primarily categorized as insoluble (70–90%) [7], SPI contains almost no insoluble soy fiber [10]. While plant-based meat analogs made exclusively from SPC can exhibit visible fibers resulting from the various naturally occurring phases in SPC, those produced solely from SPI do not possess this property. Previous researches on fiber formation in SPC products structured by HTSC were in 23–34 wt.% soy protein range. To replicate this in SPI-based analogs, a blend of 10.6 wt.% soy fiber extracted from soy flour and 33.4 wt.% SPI was proposed [5]. This mixture resulted anisotropic products characterized by fibers and layers. However, it is important to note that SPC cannot be considered a simple mixture of SPI and soy fiber, as distinct structural and mechanical properties exist [8]. Hence, incorporating insoluble fibers into SPI remains a potential area for investigation. While extensive research has been conducted by others including Grabowska et al. [9] on the structure of high-temperature short-time processed WG and SPI products, the effects of insoluble soy fiber on SPI remain largely unexplored.

This study also describes the impact of low acyl gellan gum hydrocolloid on fiber formation, in addition to insoluble soy fiber. Previous research has demonstrated that low acyl gellan gum can enhance tensile strength and promote fiber formation in pea protein isolates (PPI) and WG systems [22]. Derived from the microorganism *Sphingomonas elodea*, low acyl gellan gum has fewer acetyl side groups than native gellan, leading to increased junction zones between stacked double helices in the hydrocolloid network [14].

The outcome of this research can potentially lead to the removal of WG from plant-based meat analogs formulations, enhancing accessibility for those with celiac disease and reduce allergenicity concerns. The primary objective of this study is to gather technical insights into fiber formation in SPI-based meat analogs containing insoluble soy fiber and low acyl gellan gum at different concentrations, while excluding WG from the formula. In more detail, in this study, the impact of varying concentrations of insoluble soy fiber (ranging from 0 to 3%) and low acyl gellan gum (ranging from 0 to 2%) on the quality attributes of plant-based meat analogs composed of water, SPI, and calcium chloride will be investigated. These quality attributes will be examined through visual inspection at a macroscale, as well as at a microscale through techniques, such as confocal laser scanning microscopy (CLSM), scanning electron microscopy (SEM), and X-ray microtomography (XRT). Textural properties will be assessed by conducting rheological measurements using the closed-cavity rheometer (CCR) and by performing tensile tests. Additionally, water absorption capacity (WAC) will be determined. The study's hypotheses include that the addition of low acyl gellan gum and insoluble soy fiber will enhance the fibrous structure formed during HTSC processing with SPI, improve tensile strength, anisotropy index, air fraction, fiber formation [9, 19, 22] and WAC [1, 15].

Materials and methods

Materials

The SUPRO[®] 500E IP isolated soy protein (SPI) is a high-quality protein product with a protein content of at least 90.0 wt.%, a maximum fat content of 1.0 wt.%, and a maximum ash content of 5.0 wt.%. It was sourced from Solae (Solae Europe S.A., Switzerland, Geneva). SUPRO[®] 500E, an isolated soy protein, can improve texture, bind water, and provide gelling properties when incorporated into diverse food products, as specified by the manufacturer. The insoluble soy fiber used in this study was also obtained from Solae (Solae Europe S.A., Switzerland, Geneva). The insoluble soy fiber is composed of insoluble fiber, soluble fiber, and protein, with fiber concentrations of at least 75 wt.% and a moisture content of no more than 12 wt.%. For this study, low acyl gellan gum was used, specifically KECLOGEL[®] F Gellan gum, which was obtained from CP Kelco (CP Kelco inc, US, Atlanta). Other chemicals used in this study include calcium chloride (CaCl₂), Rhodamine B, and glutaraldehyde, all of which were obtained from Sigma-Aldrich (Germany, Darmstadt).

Methods

Preparation of different protein blends

Table 1 describes product names using abbreviations where 'F' represents insoluble soy fiber and 'G' denotes low acyl gellan gum. All blends described herein contain a formulation of 40% dry ingredients. The control dough (F0-G0) was prepared following the methods described by [18]. Figure 1 shows an overview of the preparation method of different products. First, 1 g of CaCl_2 was weighed and solubilized in 60 g of demineralized water. Then, 39 g of SPI was added and manually mixed for 2 min using a spatula. The beaker containing the dough was covered with parafilm and left to hydrate at room temperature for 30 min before transferring to the HTSC and processing.

To investigate the effect of insoluble soy fiber on the product containing SPI and CaCl_2 (F1-G0, F2-G0, and F3-G0 blends), insoluble soy fiber was added to the formulation in amounts ranging from 1 to 3%. The preparation of the dough was similar to the control dough (F0-G0), with the amount of SPI added altered to maintain a 40% dry matter content (Table 1). Specifically, an increase in insoluble soy fiber of 1, 2, or 3% decreased the SPI concentration to 38, 37, and 36%, respectively. As Fig. 1 illustrates after hydrating the dough for 30 min, the insoluble soy fiber was added, and the mixture was manually mixed and transferred to the HTSC for processing.

To evaluate the effect of low acyl gellan gum on the product containing SPI and CaCl_2 for F0-G1 and F0-G2 blends, 1 or 2% low acyl gellan gum was added. The preparation of the dough was similar to the control dough (F0-G0), with the amount of SPI added altered to maintain a 40% dry matter content (Table 1). Specifically, an increase in low acyl gellan gum of 1 or 2% decreased the SPI concentration to 38 and 37, respectively. After hydrating the dough for 30 min, low acyl gellan gum was added ranging from 1 to 2%, and the dough was mixed manually and transferred to the HTSC for processing (Fig. 1).

The final formulation group includes F1-G1, F1-G2, F2-G1, F2-G2, F3-G1, and F3-G2 blends to evaluate the effect of both insoluble soy fiber and low acyl gellan gum in the product containing SPI and CaCl_2 . In this group, 1 or 2% low acyl gellan gum was combined with 1 to 3% insoluble

Table 1 The composition of the products used in the experiments, with a constant dry matter content of 40 wt.%

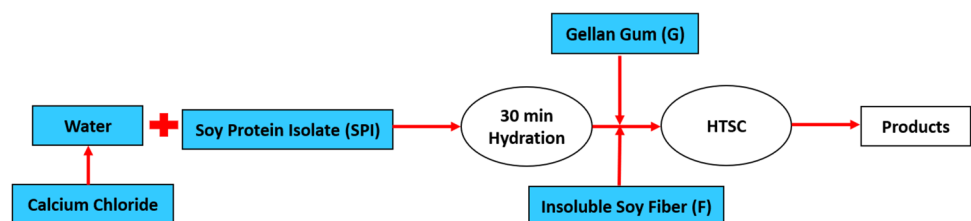
Abbreviations	Fibers (F) (wt.%)	Low acyl gellan gum (G) (wt.%)	CaCl_2 (wt.%)	Soy protein isolate (SPI) (wt.%)	Water (wt.%)
F0-G0 (Control)	0	0	1	39	60
F1-G0	1	0	1	38	60
F2-G0	2	0	1	37	60
F3-G0	3	0	1	36	60
F0-G1	0	1	1	38	60
F1-G1	1	1	1	37	60
F2-G1	2	1	1	36	60
F3-G1	3	1	1	35	60
F0-G2	0	2	1	37	60
F1-G2	1	2	1	36	60
F2-G2	2	2	1	35	60
F3-G2	3	2	1	34	60

soy fiber to maintain a 40% dry matter content (Table 1). The preparation of the dough was similar to the control dough (F0-G0), with the amount of SPI added altered to maintain a 40% dry matter content (Table 1). After hydrating the dough for 30 min, both insoluble soy fiber and low acyl gellan gum were added, and the dough was mixed manually and transferred to the HTSC for processing (Fig. 1).

High-temperature shear cell (HSTC) processing

An in-house developed batch HTSC (Wageningen University, the Netherlands) was used to process 100 g of various blends following the blend preparation detailed in previous section. The HSTC facilitated a simple shear flow by keeping the top cone stationary while the bottom cone rotated, as elucidated by Grabowska et al. [9]. The temperature in the cones and the rotation speed were controlled by circulating oil (Thermal H10, JULABO, Germany) and a Haake drive (Haake PolyLab QC, Germany), respectively [24]. The cavity (2 mm distance) between the two cones was pressurized (6.5 bar) preventing the escape of steam during processing [24]. The products were consistently maintained at an operating temperature of 120°C. A torque rheometer from

Fig. 1 Overview of the preparation method of different products



Haake Polylab QC, Germany, kept the bottom cone at a constant 30 rpm for a period of 15 min. Following this, the HTSC was cooled to 25 °C without shearing for a minimum of 10 min. The products were then removed and placed in a plastic Ziplock bag once the internal temperature of the cell dropped below 50 °C. Subsequently, the products were cooled at room temperature for at least an hour before undergoing further analysis. Then, the fresh products underwent a series of quality control measures including tensile testing, visual inspections, and examination under a reflective light microscope. The remaining products were stored at – 18 °C for later analysis. Each product was prepared and analyzed in triplicate, unless otherwise specified.

Macrostructure

The morphology of the processed products was analyzed both visually and with a reflective light microscope.

Visual inspection of the fibrous structure

To visually inspect the fibrous structure, the processed products were deformed until ruptured along the shear direction,

exposing the fibers with the longest structure (see Fig. 2A). The ruptured products were then carefully secured with a small skewer and placed in a well-lit photo booth to ensure consistent lighting conditions for photographs. The images were captured using an Apple iPhone XS with 2X zoom to capture fine details [25].

Reflective light microscope

A reflective light microscope was employed to observe the prepared products. Following the preparation process outlined in the section "Visual inspection of the fibrous structure", the products were carefully positioned beneath the Smartzoom 5× digital microscope, manufactured by Carl Zeiss Microscopy GmbH in Jena, Germany. With a magnification of 30×, detailed images of the products were captured for further analysis [21, 25].

Microstructure

In order to gain a more comprehensive understanding of the structure and alignment of the various phases present in the processed products, several microscopic techniques

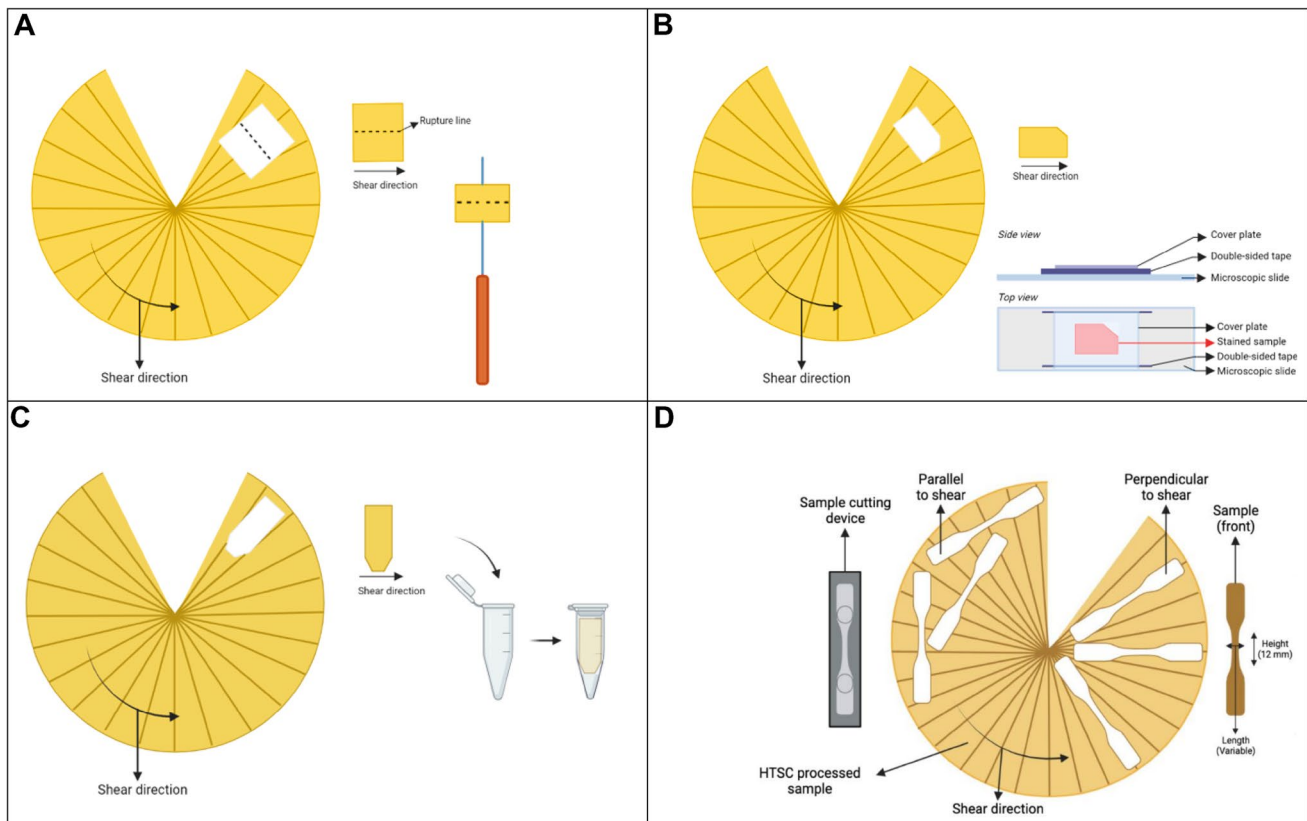


Fig. 2 Schematic overview of the sample preparation process used to determine the fibrous structure of HTSC processed products using Canon camera and SEM (A), as well as the preparation of products for CLSM (B), XRT (C), and tensile test (D)

were employed to analyze the microstructure of the products describing in the following sections:

Confocal laser scanning microscopy (CLSM)

The microstructure and the alignment of the protein phase in produced products were analyzed using confocal laser scanning microscopy (CLSM), following the procedures described by Taghian Dinani et al. [21, 23]. Frozen products were cut into trapezoids (Fig. 2B) measuring approximately 4 mm × 10 mm × 15 mm. To prepare the samples for imaging, each sample was affixed to a freezing metal plate using CryoCompound glue (Immunologic a WellMed company, Duiven, the Netherlands) and then inserted into a cryo-microtome (Micron CR50-H, ADAMAS-instruments Corp., Rhenen, the Netherlands) at − 16 °C. Thin 60 μm slices were subsequently obtained with a leveled surface, which were mounted onto a microscopic slide equipped with double-sided tape at both ends (Fig. 2B). Next, the samples were stained with a 0.002% Rhodamine B solution and covered with a cover plate before being placed in a storage container at room temperature for a minimum of 1 h. Visualization of the samples was carried out using a Confocal Scanning Laser Microscope type 510 (Zeiss, Oberkochen, Germany), equipped with a 543 nm HeNe and a 405 nm Blue/Violet diode laser, and images were captured using a 20X EC Plan-Neofluar/0.5 A lens. Subsequent image analysis was conducted using the LAS X software (Carl Zeiss Microscopy).

Scanning electron microscopy (SEM)

The microstructure (~300 μm) of the products was analyzed using SEM, following the procedure described by [6, 19, 24]. Rectangular shapes with dimensions of 13 mm × 5 mm were cut perpendicular to the shear direction from the frozen products (Fig. 2A). These samples were then soaked in tubes containing 10 mL of 2.5% (v/v) glutaraldehyde, lidded, and shaken for 8 h using a Mini Rocker-Shaker (MR1, Riga, Latvia). Afterward, the samples were rinsed with Mili-Q water and soaked in Mili-Q water overnight. To dehydrate the samples, they were soaked for 1 h in a series of ethanol solutions with increasing concentrations of 10, 30, 50, 70, 96, and 100% (v/v). Following this, the samples were dried using a critical point drier (CPD 300, Leica, Vienna, Austria) and were then ruptured parallel to the shear flow. These ruptured samples were glued using carbon cement glue and coated with 12 nm tungsten (SCD 500, Leica, Vienna, Austria). Finally, a field emission scanning electron microscope (Magellan 400, Fei, Eindhoven, the Netherlands) was used to analyze the samples with magnifications of 250X, using secondary electron detection of 13 pA and 2 kV.

X-ray microtomography

The method of X-ray microtomography (XRT) was carried out to investigate the distribution and average air volume of the products. A protocol similar to that of Jia et al. [13], Schreuders et al. [18] and Taghian Dinani et al. [23] was followed. Rectangular-shaped frozen samples with dimensions of 8 mm × 20 mm were taken, and two corners were cut to fit in a 2 mL Eppendorf tube (Fig. 2C). The tube was then placed in a microCT system phoenix Vltomelx m (GE Sensing & Inspection Technologies GmbH, Wunstorf, Germany), positioned 23.43 μm from the X-ray source, resulting in a spatial resolution of 6 μm. A voltage of 75 kV and a current of 80 μA were applied to the focus tube, and 1500 photos were taken with steps of 0.24° around the sample to achieve a 360° view of the sample. The pictures were reconstructed by the GE reconstruction software (GE, Wunstorf, Germany) to obtain one single 3D object. Then, the reconstructed images were analyzed with Avizo imaging software to obtain data on total volume, void volume, length 3D, and width 3D in the samples. Each product was measured in duplicate by XRT.

Textural properties

The textural properties of the products were assessed via a tensile test, whereas a CCR measurement was performed to simulate processing conditions and gauge their impact on the blends.

Rheological properties

To investigate the structure formation and characterize the rheological properties of the dough during thermomechanical processing, a time-sweep measurement was conducted at 120°C using a closed-cavity rheometer (CCR) (RPA, TA Instruments, New Castle, DE, USA) [17]. The procedure started with a stationary step in which about 5 g of the dough prepared in the section "Preparation of different protein blends" was placed between two plastic foils and then sealed at 4 bar pressure for 2 min to prevent water evaporation. Subsequently, a constant strain of 80% and a frequency of 10 Hz were applied to the sample for 15 min in an isothermal measurement. Next, the temperature was gradually reduced to 40 °C at a cooling rate of 5°C/min, while keeping other variables constant. Storage (G') [kPa] and loss modulus (G'') [kPa] were determined from this test. Loss tangent ($\tan \delta$) [–] at the end of both heating and cooling steps was then calculated from the G' and G'' values using Eq. 1:

$$\tan \delta = \frac{G''}{G'} \quad (1)$$

Tensile strength analysis

The mechanical properties of the products were evaluated using a Texture analyzer (TA.XTPlusC). Approximately one hour after the preparation of the products, they were cut by a bone-shaped tensile bar (Fig. 2D). To determine the tensile stress (σ) [N/m^2], width, height, and length parameters of tensile bars were measured using a digital caliper (Mitutoyo, Kawasaki, Japan). Subsequently, the samples were placed in the texture analyzer, where the two ends were clamped to secure them in place. Uni-axial tension tests were conducted until failure with a constant deformation rate of 1 mm/s, as described by Schlangen et al. [16] and Taghian Dinani et al. [24]. The samples were also tested parallel and perpendicular to the shear flow direction to determine the degree of anisotropy. The force [N] required to rupture the sample was recorded by the Exponent Connect Software (Stable Micro Systems, UK). The tensile stress, σ , was calculated by dividing the fracture stress (F_t [N]) by the initial area (A_0 [m^2]) of the sample. To calculate the tensile strain (ε [-]), the bone-shaped tensile bar height at time t (h_t) was divided by its initial height of 15.5 mm (h_0). The results of tensile stress (σ) in parallel and perpendicular tests calculated by Eq. 2 were combined to determine the anisotropic index (AI) for tensile stress, which was calculated using Eq. 3 [6]:

$$\sigma = \frac{F_t \times h_0}{A_0 \times h_t} \quad (2)$$

$$\text{AI}(\sigma) = \frac{\sigma_{\text{parallel}}}{\sigma_{\text{perpendicular}}} \quad (3)$$

Technological property of water absorption capacity (WAC)

The WAC was determined to assess the amount of water absorbed by the products following the procedure outlined by Taghian Dinani et al. [21, 23]. Frozen products were uniformly cut into 1 cm diameter circles to ensure consistent thickness and weight before hydration. Subsequently, these samples were weighed (W_{bh}) and placed in a small plastic cup containing 25 mL of deionized water, and positioned in a water bath (JULABO, Germany) set at 50 °C for 16 h. Following the incubation period, the samples were removed from the cups, allowed to air-dry for 5 min at room temperature, and weighed after hydration (W_{ah}). WAC was calculated using Eq. 4.

$$\text{WAC} = \frac{W_{\text{ah}} - W_{\text{bh}}}{W_{\text{bh}}} \times 100 \quad (4)$$

Statistical analysis

In this study, data analysis was conducted using SPSS statistical software (Version 28.0.1.1., IBM, Armonk, NY) through the application of the general linear model (GLM) procedure. The dependent variables underwent homogeneity tests, followed by regression analysis and analysis of variance (ANOVA) using the GLM. When significant differences were detected among the means of the dependent variables at a significance level of 95% ($p \leq 0.05$), Duncan's test was employed. The results are reported as mean \pm standard deviation (SD).

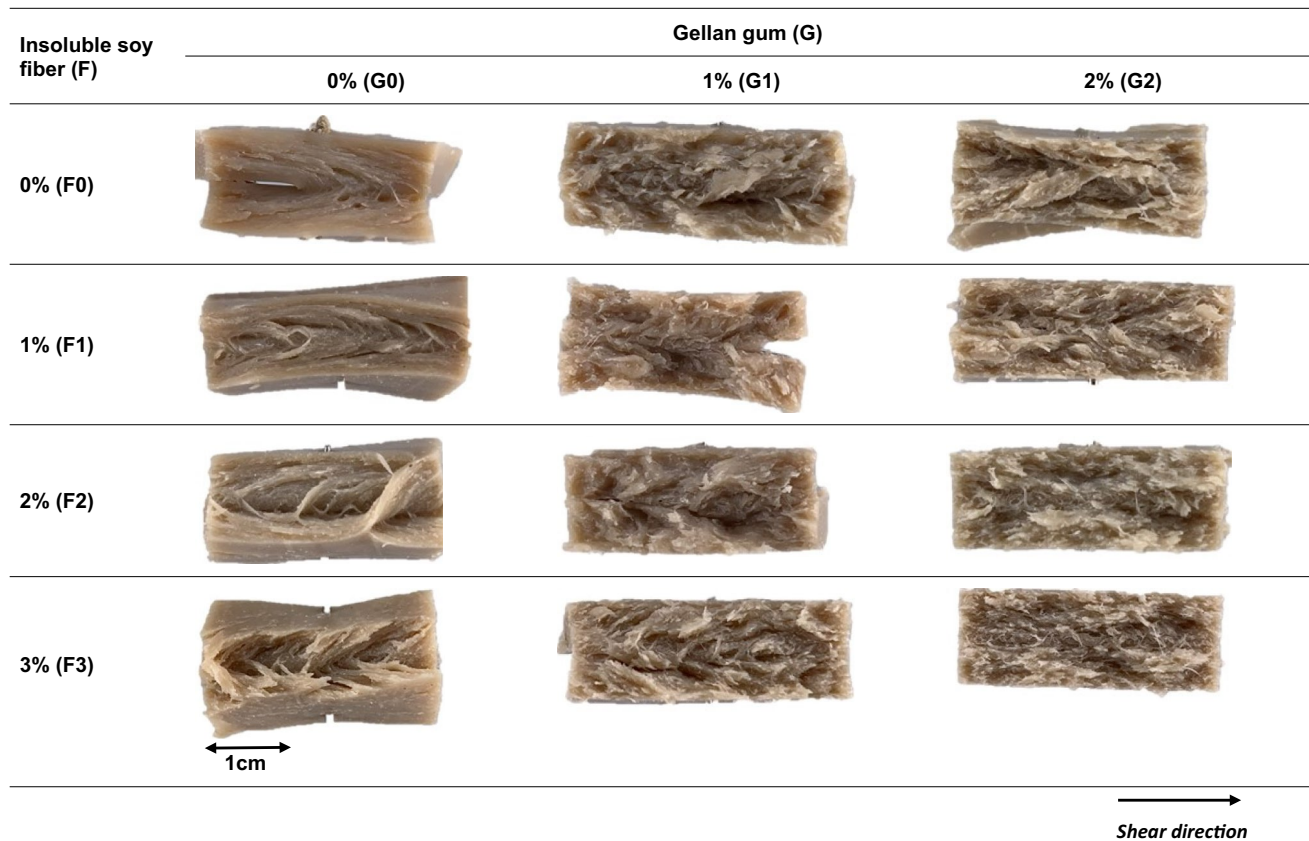
Results and discussion

Macrostructure

Visual inspection

To assess the structure, the products underwent intentional rupture by folding them in a direction aligned with the shear flow. This orientation was chosen to potentially unveil the longest elongated fibers within products created using various formulations outlined in Table 1. As illustrated in Table 2, the utilization of the control formulation (F0-G0) did not yield a fibrous product. Instead, a product with a more layered structure was observed, and F0-G0 exhibited substantial resistance to bending, rendering it a firm, dense gel. The surface of the F0-G0 was smooth and devoid of brittleness, consistent with previous research findings [8, 19]. This outcome was attributed to the composition of SPI, which contains minimal components beyond protein to form a dispersed phase [2]. Fiber formation was explained by the deformation of the dispersed droplets entrapped within the continuous protein phase, occurring in the direction of shear flow, as reported by Dekkers et al. [5] and Taghian Dinani et al. [22].

However, the introduction of low acyl gellan gum into formulations devoid of insoluble soy fibers (F0), such as F0-G1 and F0-G2, yielded small, thin, and short fibers (Table 2). Nonetheless, these products exhibited increased brittleness compared to the control (F0-G0). It was expected that the addition of low acyl gellan gum to the formulation would foster fiber formation, given its lower concentration relative to the SPI content, making it conducive to forming the dispersed phase. Prior research by Taghian Dinani et al. [22] demonstrated that low acyl gellan gum, when combined with pea protein isolate (PPI) and WG, produced a clearer fibrous structure. It was hypothesized that low acyl gellan gum formed an additional dispersed phase by constructing stacked helices, stabilized by Ca^{2+} ions upon gelation in the PPI-WG blends [22]. Table 2 exhibits that the incorporation

Table 2 Overview of the macrostructure of plant-based meat alternatives with and without the addition of insoluble soy fiber (F) and/or low acyl gellan gum (G)

Pictures were taken using an iPhone XS with 2X zoom. The ruptured samples were secured along their shear direction with a small skewer and placed in a well-lit photo booth to capture their images

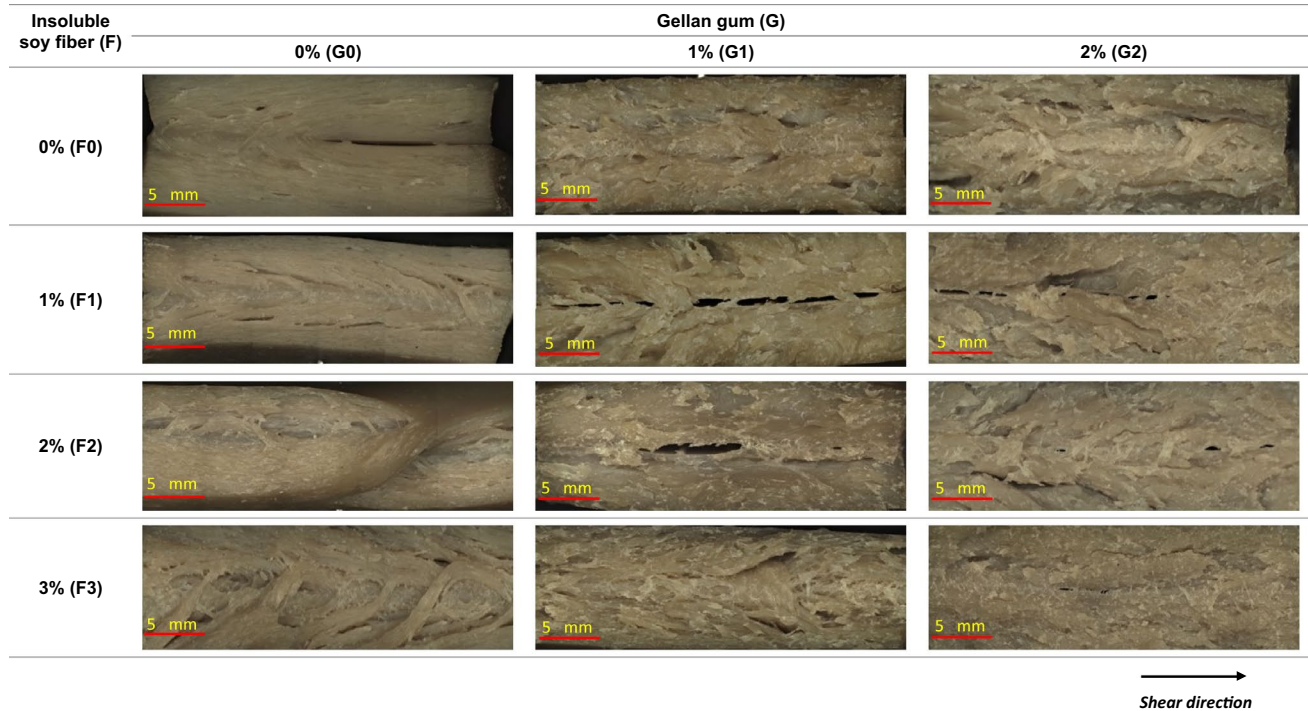
of insoluble soy fiber in F1-G0, F2-G0, and F3-G0 formulations led to the development of a fibrous structure, characterized by visibly long and thick fibers. In comparison to F0-G0, these products exhibited heightened compactness and density, rendering them less prone to rupture. It is noteworthy that these products necessitated complete folding before any rupture could occur.

Table 2 reveals that the incorporation of insoluble soy fiber and low acyl gellan gum did not yield lengthy and elongated fibers. In comparison to the control product (F0-G0), F1-G1, F1-G2, F2-G1, F2-G2, F3-G1, and F3-G2 products displayed only thin and short fibrils, slightly oriented in the shear direction. Among the products containing a blend of low acyl gellan gum and insoluble soy fiber, those with 1 wt.% low acyl gellan gum (F1-G1, F2-G1, and F3-G1) appeared to possess larger fibrils than those with 2 wt.%. Nonetheless, all these products exhibited brittleness, with increasing concentration of low acyl gellan gum and insoluble soy fiber resulting in weaker products prone to rupture under stress induced by manual bending. This trend was also evident in the results of the tensile test, as will be discussed in the section "[Tensile test](#)". In summary, the addition of

insoluble soy fiber to SPI blends resulted in products with a fibrous and layered structure, consistent with the hypothesis proposed by Grabowska et al. [9]. Meanwhile, the addition of low acyl gellan gum resulted in a product characterized by increased fibrillation and increased brittleness. However, the combination of low acyl gellan gum and insoluble soy fiber resulted in the formation of short and thin fibers.

Smartzoom pictures

To examine the macrostructure of the products further, photographs were captured using the Smartzoom 5X, and as indicated in Table 3, the control product (F0-G0) exhibited a layered structure rather than a fibrous one, with a solid and gel-like appearance. These observations are consistent with the outcomes discussed in the previous section. Similarly, formulations F0-G1 and F0-G2 exhibited only short fibrillar filaments and the products were very brittle, as illustrated in Table 3. These findings align with the earlier findings described in the previous section. Table 3 illustrates that the addition of insoluble soy fiber, as represented by F1-G0, F2-G0, and F3-G0, led to the formation of visible fibers. Specifically, F1-G0 displayed

Table 3 Overview of the macrostructure of plant-based meat alternatives with and without the addition of insoluble soy fiber (F) and/or low acyl gellan gum (G)

Pictures were taken using a Smartzoom 5× digital microscope with a magnification of 30×

thin fibers that were aligned in the direction of shear flow, along with a layered structure. Similarly, F2-G0 exhibited a fibrous and layered structure that was aligned in the direction of shearing. On the other hand, F3-G0 had the thickest fibers among all the products, also aligned in the shearing direction. However, its structure was more brittle and prone to rupture compared to F1-G0 and F2-G0. Images of products containing both insoluble soy fiber and low acyl gellan gum, including F1-G1, F1-G2, F2-G1, F2-G2, F3-G1, and F3-G2, revealed short and thin fibrous structures that were brittle and oriented in the shear direction. These observations are consistent with the findings presented earlier in the previous section. According to Taghian Dinani et al. [22], the incorporation of low acyl gellan gel led to the production of fibers in PPI/WG blend. Similarly, Schreuders et al., [19] illustrated the development of a fibrous structure within SPI by incorporating both soluble pectin fibers and insoluble cellulose fibers. Our research aligns with these prior observations, emphasizing the possibilities of enhancing blends and composites with low acyl gellan gum and insoluble fibers.

Microstructure

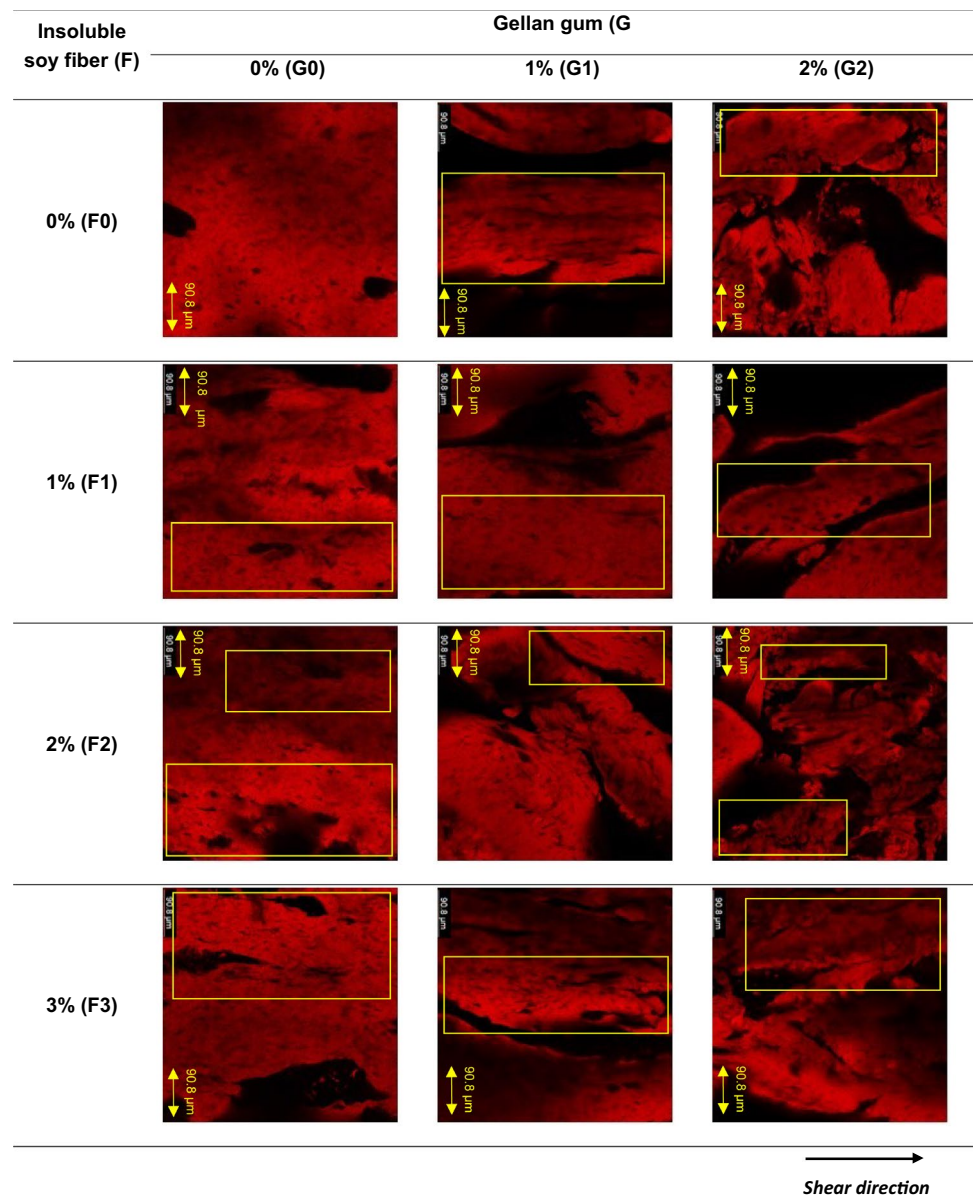
CLSM

Confocal Laser Scanning Microscopy (CLSM) was performed on all formulations listed in Table 1 in the

direction of shear flow. Rhodamine B staining was used to distinguish between protein and non-protein regions in the products, as depicted in Table 4. The control product (F0-G0) displayed fewer dark areas, indicating the absence of components beyond SPI. The black areas observed in the products indicate the presence of either water or air, as neither insoluble soy fiber nor low acyl gellan gum was added. Spherical-shaped black spots were also visible in the control product (F0-G0). Conversely, the smooth red regions in products F1-G0, F2-G0, and F3-G0 exhibited elliptical-shaped black spots in the shear flow direction, signifying the impact of shear direction on structure formation. This effect was less pronounced in the F0-G0 product, where no fibers were present, as confirmed in Tables 2, 3, and 4.

The addition of 1, 2, and 3 wt.% of insoluble soy fiber (F1-G0, F2-G0, and F3-G0) resulted in darker regions compared to F0-G0, indicating the presence of another phase, such as water, air, or insoluble soy fiber. Table 4 displays yellow rectangles that represent regions aligned with the shear direction, corresponding to the darker regions stretched in the shear direction observed in products F1-G0, F2-G0, and F3-G0. This aligns with the visual observation of fibers in products F1-G0, F2-G0, and F3-G0 in Tables 2 and 3. X-ray Tomography (XRT) measurements in Table 6 indicated that the air inclusions in products F1-G0, F2-G0, and F3-G0 exhibited a more elliptical shape, consistent with the

Table 4 Overview of CLSM images of the microstructure of plant-based meat alternatives with and without addition of insoluble soy fiber (F) and/or low acyl gellan gum (G)



Yellow rectangles indicate orientation in the samples in shear flow direction. Visualization of the samples was carried out using a Confocal Scanning Laser Microscope type 510 equipped with a 543 nm HeNe and a 405 nm Blue/Violet diode laser, and images were captured using a 20× EC PlanNeofluar/0.5 A lens

small, stretched black regions found in pictures containing insoluble soy fiber in Table 4.

The incorporation of low acyl gellan gum (F0-G1, F1-G1, F2-G1, F3-G1, F0-G2, F1-G2, F2-G2, and F3-G2) resulted in more dark areas in all products compared to those without low acyl gellan gum (F0-G0, F1-G0, F2-G0, and F3-G0). Voids present in products containing low acyl gellan gum displayed a more irregular shape than those in products F0-G0, F1-G0, F2-G0, and F3-G0. In a previous study [21], PPI:WG mixtures containing hydrocolloids showed darker regions in most products compared to the

control, likely due to elongated air bubbles or hydrocolloid-only domains. This aligns with the findings of our current study. Notably, products containing both insoluble soy fiber and low acyl gellan gum (F1-G1, F2-G1, F3-G1, F1-G2, F2-G2, and F3-G2) resembled products with only low acyl gellan gum addition (F0-G1 and F0-G2). The inclusion of low acyl gellan gum resulted in the formation of smaller filaments on a small scale, monitoring the smaller filaments observed on a macro-scale in Tables 2 and 3.

SEM

SEM analysis was employed to examine the microstructure of plant-based meat analogs across all the formulations detailed in Table 1. In products containing solely SPI (F0-G0), the voids took on spherical appearance, suggesting that the shearing process had a limited impact on SPI orientation (Table 6). The surface of product F0-G0 exhibited a relatively smooth texture, in stark contrast to products containing low acyl gellan gum (F0-G1, F1-G1, F2-G1, F3-G1, F0-G2, F1-G2, F2-G2, and F3-G2), which displayed noticeable roughness. However, when compared to products containing insoluble soy fiber (F1-G0, F2-G0, and F3-G0), F0-G0 displayed a moderate level of roughness. This smoothness was also evident at a macro-scale in Tables 3 and 4, where the products exhibited limited layers. Similar findings were obtained by Grabowska et al. [8] using a 30 wt.% SPI formulation processed at 95 °C.

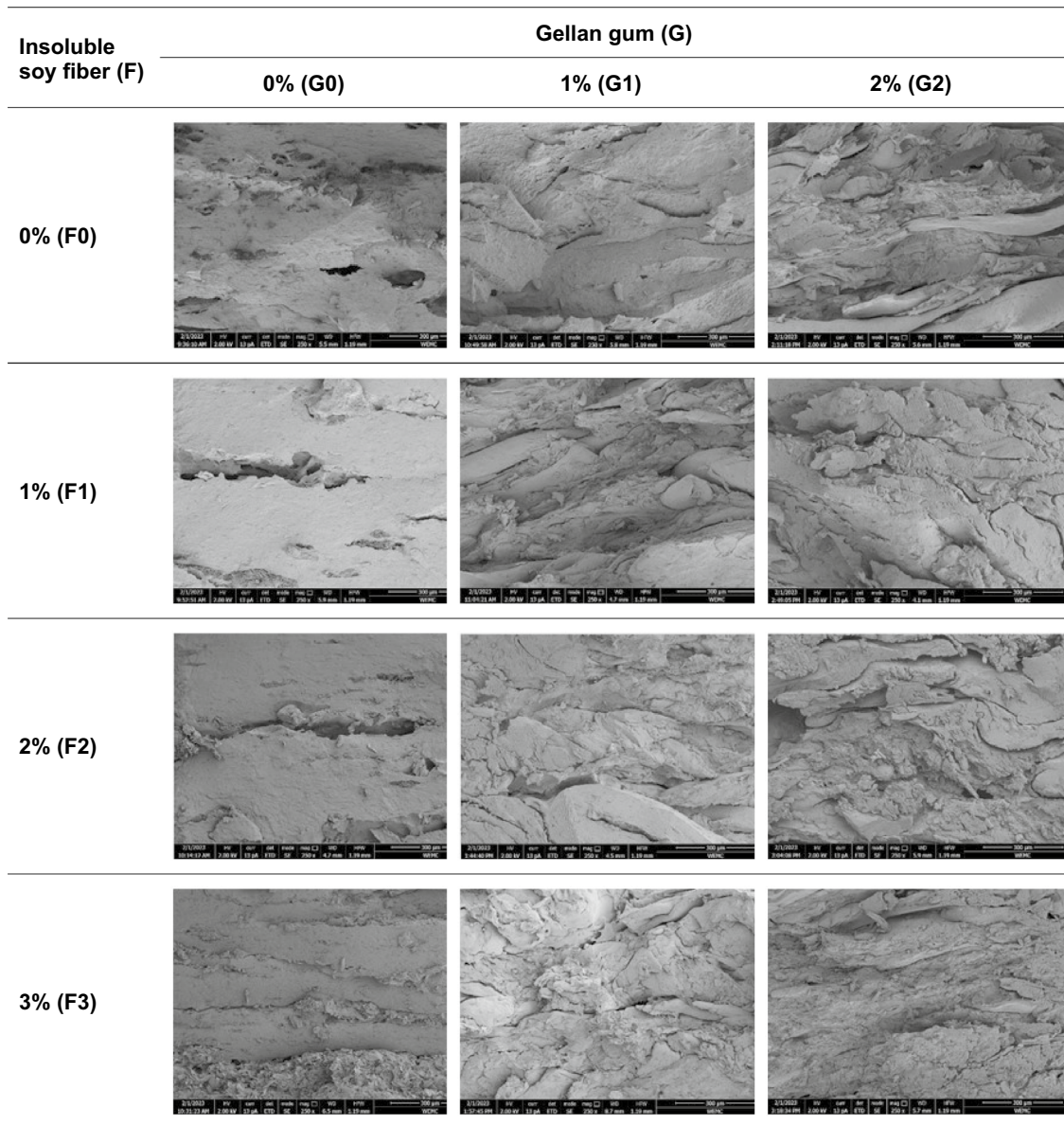
SEM images revealed that products containing insoluble soy fiber, specifically F1-G0, F2-G0, and F3-G0, exhibited the smoothest microstructural regions, with F1-G0 being the smoothest among all the products (as indicated in Table 6). However, with an increase in insoluble soy fiber concentration, a visible phase separation became apparent, resulting in less smooth surfaces. This indicates that the addition of 1–2% insoluble soy fiber to SPI initiates the formation of a distinct phase. Furthermore, an anisotropy index was highest for the aforementioned products (F1-G0, F2-G0, and F3-G0) in Fig. 5A, consistent with the presence of elongated voids in the shear direction observed in the XRT images in Table 6.

The addition of low acyl gellan gum in the products (F0-G1, F1-G1, F2-G1, F3-G1, F0-G2, F1-G2, F2-G2, and F3-G2) resulted in the formation of short and disrupted filaments, with filament size decreasing with increasing concentrations of insoluble soy fiber and low acyl gellan gum. These observations aligned with those in Tables 3 and 4, which demonstrated that the products containing low acyl gellan gum displayed short fibrillar filaments upon fracturing. Furthermore, the filaments in these products exhibited alignment in the shear direction, indicating stretching of the filaments in that direction. This alignment was consistent with the CLSM images presented in Table 5, showcasing a general orientation of the protein phase in the shear flow direction, along with short and disrupted filaments. Products containing low acyl gellan gum (G1 and G2) exhibited more phase separation than F1-G0, F2-G0, and F3-G0, with many regions exhibiting a rough surface that increased with increasing concentrations of insoluble soy fiber and low acyl gellan gum. However, in contrast to the insoluble soy fiber-containing products, no voids with an alignment in the shear direction were observed in the products containing low acyl gellan gum, as confirmed by the XRT pictures presented in Table 6.

XRT

Table 6 and Table S1 (in the Appendix section) display 3D X-ray microtomography (XRT) images that depict the air inclusions and solid parts of the products. Additionally, Fig. 3 and Figure S1 (in the Appendix section) illustrate the air fraction and average bubble volume of the products. Table 6 and Fig. 3 demonstrate that product F0-G0 had an air fraction of $4.10 \pm 0.03\%$, which was significantly lower ($p \leq 0.05$) than the products that contained insoluble soy fiber (F1-G0, F2-G0, and F3-G0), but significantly higher ($p \leq 0.05$) than the products that contained low acyl gellan gum (F0-G1, F1-G1, F2-G1, F3-G1, F0-G2, F1-G2, F2-G2, and F3-G2). This highlights the ability of the control product to retain air and the fact that this ability is influenced by the addition of soy fiber and low acyl gellan gum. Previous studies on SPI have also demonstrated its ability to retain air [3, 4]. Among the products containing insoluble soy fiber, it was observed in Fig. 3 that the air fraction ($7.54 \pm 1.29\%$, $7.55 \pm 0.28\%$, and $6.18 \pm 0.50\%$ for F1-G0, F2-G0, and F3-G0, respectively) was significantly higher ($p \leq 0.05$) than all the other products. In addition, these products displayed the highest average bubble volume values as shown in Figure S1 of the Appendix section. Thus, insoluble soy fiber was found to improve the air-retaining ability. This aligns with previous research on SPI + pectin, which found that the air fraction of the products increased with the addition of a second phase [3, 4]. Similar findings have been reported in studies using other raw materials, such as calcium caseinate. However, research on calcium caseinate further found that incorporating air into the material resulted in a fibrous appearance and enhanced the anisotropy of sheared products [28].

The incorporation of low acyl gellan gum (F0-G1, F1-G1, F2-G1, F3-G1, F0-G2, F1-G2, F2-G2, and F3-G2) had a discernible impact on the distribution and morphology of the air bubbles (as indicated in Table 6). In contrast to the products containing insoluble soy fiber (F1-G0, F2-G0, and F3-G0), the bubbles in the low acyl gellan gum-containing products seemed to be randomly distributed and exhibited highly irregular shapes. Additionally, at the macroscopic level (as illustrated in Tables 2 and 3), these products displayed short and irregular filaments. These observations suggest some degree of phase alignment in the direction of shear flow for the low acyl gellan gum-containing products (F0-G1, F1-G1, F2-G1, F3-G1, F0-G2, F1-G2, F2-G2, and F3-G2), although the effect was not as prominent as that observed in the products containing insoluble soy fiber (F1-G0, F2-G0, F3-G0). This finding was further corroborated by the CLSM and SEM images, which showed no special distinct orientation in the shear flow direction of low acyl gellan gum-containing products (as depicted in Tables 5 and 6, respectively).

Table 5 Scanning electron microscopic (SEM) images of cross sections from plant-based meat alternatives pictures for samples with and without the addition of insoluble soy fiber (F) and or low acyl gellan gum (G) observed at 250× magnification

→
Shear direction

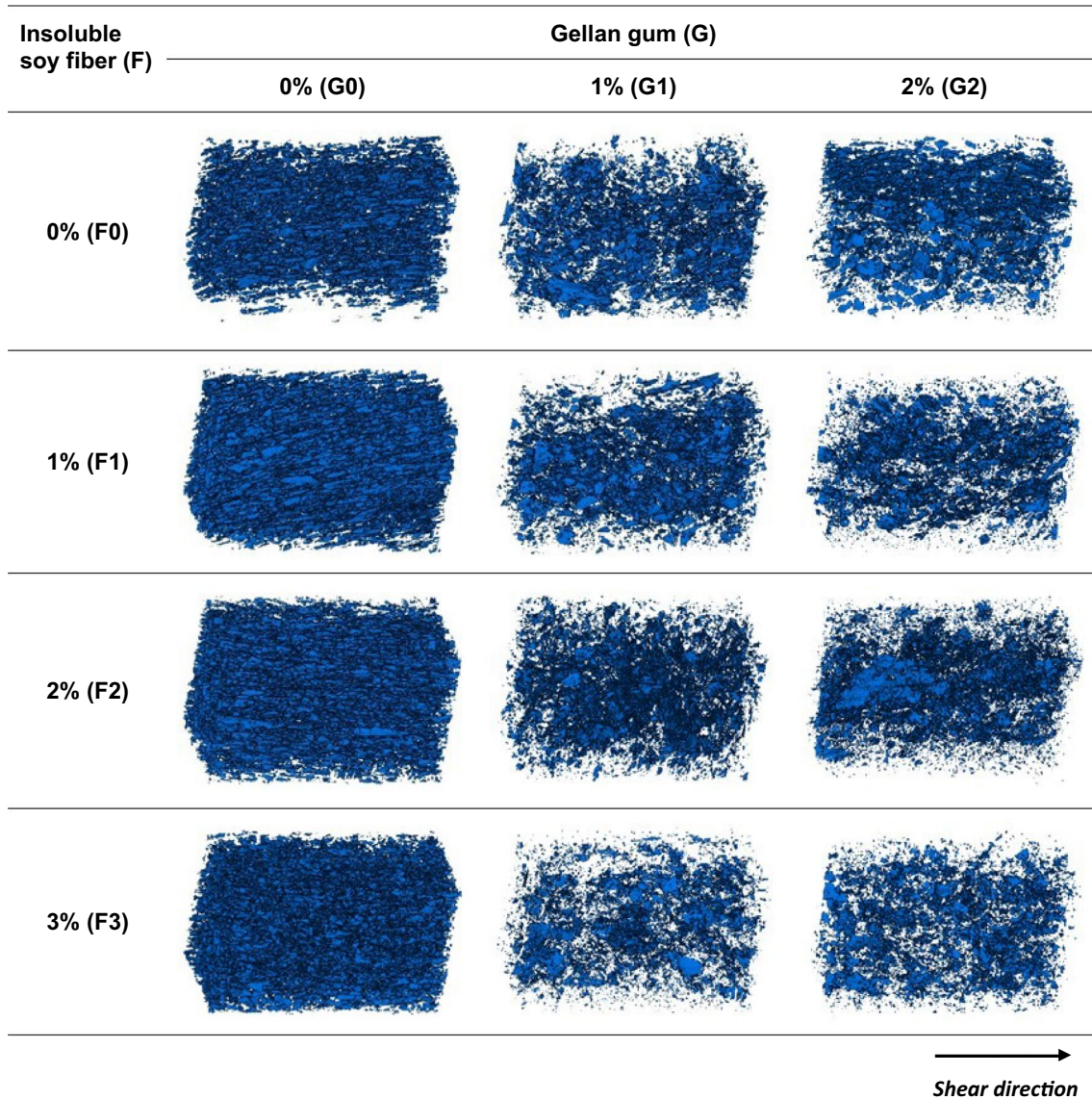
Prior to taking pictures, samples were fixed with glutaraldehyde, dried with a critical point drier, and ruptured parallel to the shear flow

These results are consistent with previous findings that emphasize the significance of the air phase in providing structure by arranging protein fibers in the direction of shear flow to produce a fibrous, mechanically anisotropic material [3, 28]. The addition of low acyl gellan gum did not lead to the aforementioned observations, thereby emphasizing the importance ingredients to be able to incorporate air when aiming for fibrous and anisotropic material.

Textural properties

Rheological properties

The viscoelastic characteristics of all formulations, as shown in Table 1, were determined using a time-sweep measurement technique utilizing the CCR. The loss tangent ($\tan \delta$), which is the ratio of G'' to G' , was used to assess the properties of the material. A high $\tan \delta$ indicates a more viscous

Table 6 3D X-ray microtomography (XRT) images with a spatial resolution of 6 μm representing air inclusion in HTSC plant-based meat alternatives with and without the addition of insoluble soy fiber (F) and or low acyl gellan gum (G)

material, while a low $\tan \delta$ indicates a more elastic material that can store more energy. The results of the $\tan \delta$ measurements obtained at the conclusion of both the heating and cooling processes are illustrated in Fig. 4. Furthermore, Figure S2. A and B in the Appendix section displays the G' and G'' values of the products at the conclusion of both the heating and cooling phases, respectively, of the time-sweep test.

At the conclusion of the heating process, F0-G0 exhibited the most elastic behavior, as evidenced by its lowest $\tan \delta$ value (Fig. 4). The addition of insoluble soy fiber (F1-G0, F2-G0, and F3-G0) produced a significant ($p \leq 0.05$) increase in viscosity, as evidenced by the higher $\tan \delta$ value (and Figure S2.A in Appendix) in comparison to F0-G0. The inclusion of low acyl gellan gum in the products (F0-G1, F1-G1, F2-G1, F3-G1, F1-G2, F2-G2, and F3-G2) resulted

in an increase in $\tan \delta$, indicating that these products were less elastic and more have more viscous behavior following heating and shearing. This outcome could be attributed to the higher viscosity increase imparted by low acyl gellan gum compared to insoluble soy fiber, resulting in a more pronounced increase in viscosity in products that contained low acyl gellan gum, either alone or in combination with insoluble soy fiber [14].

Following the heating and shearing process in the CCR, the products were cooled to 25 °C for 7.5 min, which is typically referred to as the region where the product structure becomes fixed. As shown in Fig. 4, products containing only insoluble soy fiber (F1-G0, F2-G0, and F3-G0) exhibited significantly lower $\tan \delta$ values ($p \leq 0.05$) after cooling compared to products containing low acyl gellan gum

Fig. 3 Air fraction of HTSC processed products with and without the addition of insoluble soy fiber (F) and or low acyl gellan gum (G) obtained from data analysis of 3D X-ray microtomography (XRT) images. In this figure, data are represented as mean \pm SD and different English letters show statistically significant difference of data ($p \leq 0.05$)

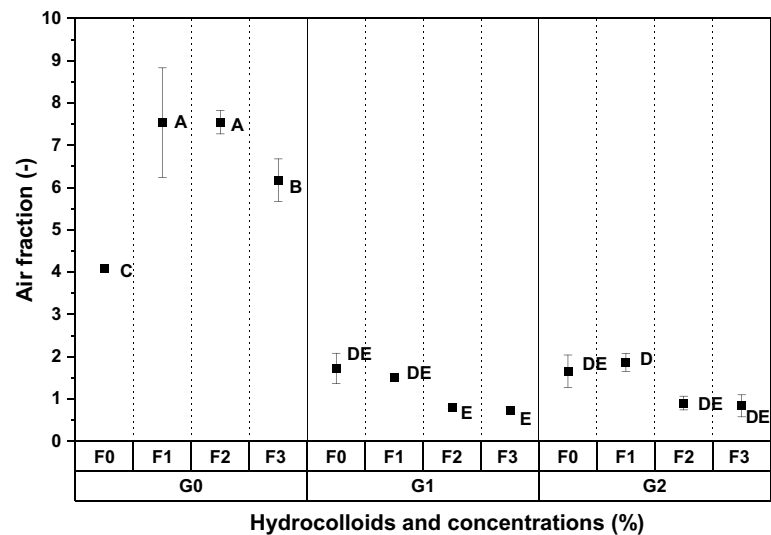
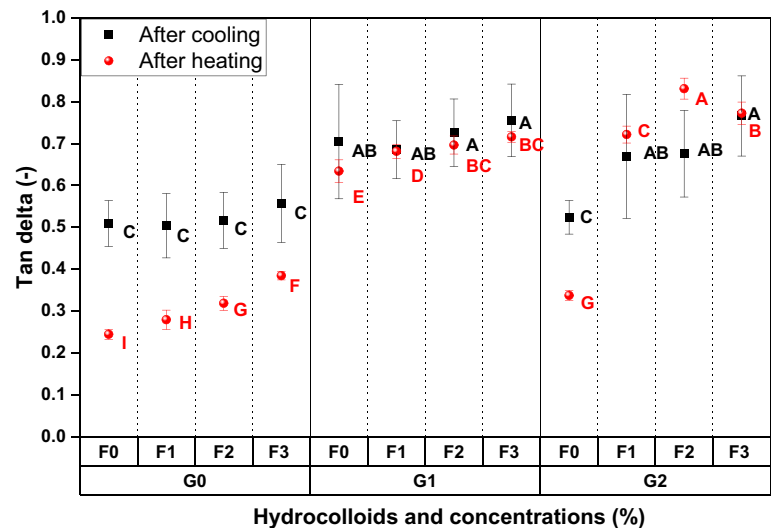


Fig. 4 The development of tan δ over time sweep measurements after heating (●) (15 min, 120 °C, 80% strain, 10 Hz) and after cooling (■) (7.5 min, 25 °C, 0% strain, 0 Hz) for all formulations with and without the addition of insoluble soy fiber (F) and or low acyl gellan gum (G). In this figure, data are represented as mean \pm SD and different English letters show statistically significant difference of data ($p \leq 0.05$)

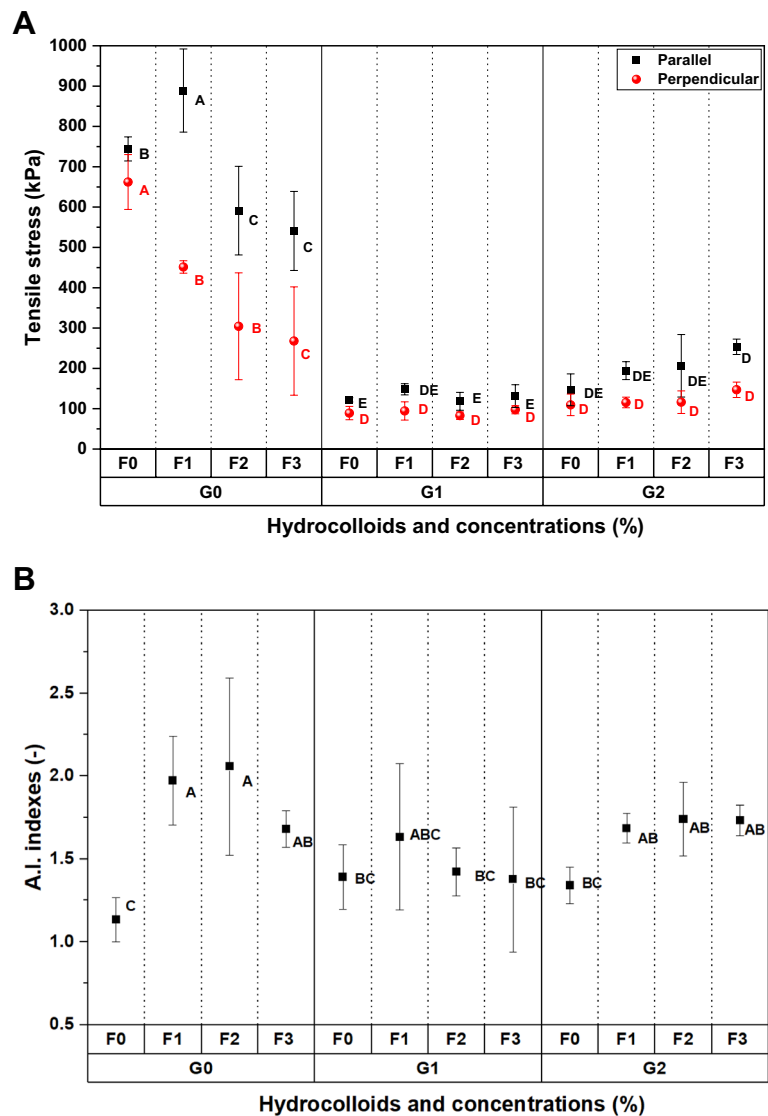


(F0-G1, F1-G1, F2-G1, F3-G1, F1-G2, F2-G2, and F3-G2), indicating greater elasticity. This finding is consistent with the textural properties discussed in the next section, which revealed that products containing only insoluble soy fiber exhibited higher values of tensile stress when tested using a texture analyzer (Fig. 5). Despite displaying similar rheological properties to the control product (F0-G0), products F1-G0, F2-G0, and F3-G0 exhibited visible fibers, whereas the control product did not (Tables 2 and 3).

The addition of low acyl gellan gum to the products (F0-G1, F1-G1, F2-G1, F3-G1, F1-G2, F2-G2, and F3-G2) resulted in a higher value of tan δ compared to the control and the products containing only insoluble soy fiber (F0-G0, F1-G0, F2-G0, and F3-G0). This indicated that the products containing low acyl gellan gum were less elastic and more viscous, resulting in less brittle gels. These observations were consistent with the results of visual inspection shown in Tables 2 and 3, which showed that the products

containing low acyl gellan gum were very brittle. Moreover, these findings were supported by the results discussed in the next section, which showed a significant decrease ($p \leq 0.05$) in tensile stress when low acyl gellan gum was added to the formulations. The presence of low acyl gellan gum made the products more liquid-like, which may explain the decrease in apparent G' observed after heating in F0-G1, F1-G1, F2-G1, F3-G1, F1-G2, F2-G2, and F3-G2 (Figure S2.A in Appendix section), as cross-links formed between protein molecules may be hindered by the presence of low acyl gellan gum. The observed increase in tan δ to around 1 indicated a decrease in gel stiffness for the products containing low acyl gellan gum (F0-G1, F1-G1, F2-G1, F3-G1, F1-G2, F2-G2, and F3-G2), suggesting that there were fewer or weaker bonds between molecules in the product. It was hypothesized that low acyl gellan gum and SPI may not have similar rheological properties under the process conditions in the HTSC, which may explain why no fibrous structure

Fig. 5 **A** The tensile stress for products with and without the addition of insoluble soy fiber (F) and or low acyl gellan gum (G) sheared for 15 min, 30 rpm at 120°C deformed in parallel (■) and perpendicular (●) direction. **B** The anisotropy index (AI)(-) stress of the products. In this figure, data are represented as mean \pm SD and different English letters show statistically significant difference of data ($p \leq 0.05$)



was observed. Moreover, it could show that low acyl gellan gum is not chemically stable and that it might hydrolyze upon processing.

Tensile test

Tensile tests were conducted on all the formulations listed in Table 1, in both parallel and perpendicular directions to the shear flow. The shear stress and the AI values based on shear stress are depicted in Fig. 5A and B, respectively. Moreover, the Young's moduli are shown in Figure S3 in Appendix section. The tensile stress values were very similar for both parallel and perpendicular directions in case of the control products (F0-G0) (Fig. 5A), suggesting that the product exhibited isotropic behavior. This finding was further supported by the AI values shown in Fig. 5B, where AI was close to 1. Moreover, no visible fibers were observed in

the product at a macro-scale, as presented in Tables 2 and 3. As a result, the strength of the gel was less reliant on being subjected to stress in either the parallel or perpendicular direction, but rather on its overall strength as a gel. This non-orientation-dependent behavior was confirmed through other imaging techniques, including CLSM images (Table 4) and SEM (Table 5), which indicated that there was only minor orientation of the F0-G0 product in the shear direction, appearing as layers.

In the case of formulation F1-G0, it was observed that the tensile stress was significantly higher ($p \leq 0.05$) in the parallel direction compared to the perpendicular direction, with values of 889 ± 103 kPa and 451 ± 153 kPa, respectively (as shown in Figs. 5A). These values for tensile stress were the highest among all the tested products except for the perpendicular direction when compared to the control product (F0-G0). These results suggest that

the addition of 1 wt.% insoluble soy fiber increased the strength of the material, while also causing enough phase separation to allow for fiber formation. The higher tensile stress observed in the parallel direction also suggests the presence of anisotropy in the product (as shown in Fig. 5B). This observation aligns with the macro-scale observation of visible fibers oriented in the shear direction. Additionally, the anisotropic behavior was evident even at the micro-scale, as demonstrated by the CLSM and SEM images that displayed the product being oriented in the shearing direction (as presented in Tables 4 and 5, respectively). In previous research conducted by Schreuders et al. [19], it was discovered that HTSC processing of mixtures consisting of 41 wt.% SPI, 1.5 wt.% pectin, and 1.5 wt.% cellulose resulted in tensile stress values of approximately 850 ± 250 kPa in the parallel direction and 550 ± 125 kPa in the perpendicular direction. These values were attributed to the presence of fibers and the level of elongation of the dispersed phase, which is consistent with the results of this study that also identified a fibrous structure and a higher degree of mechanical anisotropy.

The results obtained from the experiments conducted on F2-G0 and F3-G0 products indicate a noteworthy ($p \leq 0.05$) reduction in tensile stress (304 ± 132 kPa and 268 ± 134 kPa perpendicular, 591 ± 109 kPa and 541 ± 98 kPa parallel, respectively) in comparison to F1-G0 (refer to Fig. 5A). Despite this decline, the values of tensile stress remained considerably higher ($p \leq 0.05$) than the products containing low acyl gellan gum (F0-G1, F1-G1, F2-G1, F3-G1, F0-G2, F1-G2, F2-G2, and F3-G2). Moreover, the tensile stress values were greater in the parallel direction than in the perpendicular direction, indicating the anisotropic behavior of the products, as shown in Fig. 5B. This observation was confirmed by the presence of visible fibers in the products at a macroscopic level (refer to Tables 2 and 3) and the orientation of the products in the shearing direction at a microscopic level, as demonstrated in the CLSM (refer to Table 4) and SEM images (refer to Table 5). These findings are consistent with the observations that products containing insoluble soy fiber exhibited greater resistance to rupture upon bending compared to products containing low acyl gellan gum. Specifically, products identified as F0-G1, F1-G1, F2-G1, F3-G1, F0-G2, F1-G2, F2-G2, and F3-G2 demonstrated this trend. This implies that insoluble soy fiber has the capacity to enhance the material's strength while promoting phase separation, which results in the formation of visible fibers along the shear flow direction. In addition, an increase in the concentration of insoluble soy fiber led to a less elastic and more viscous behavior, as illustrated in Fig. 4, which corresponds with the decreasing trend in tensile stress (Fig. 5A).

The other products containing low acyl gellan gum, specifically F0-G1, F1-G1, F2-G1, F3-G1, F0-G2, F1-G2, F2-G2, and F3-G2 displayed slightly higher tensile stress values in

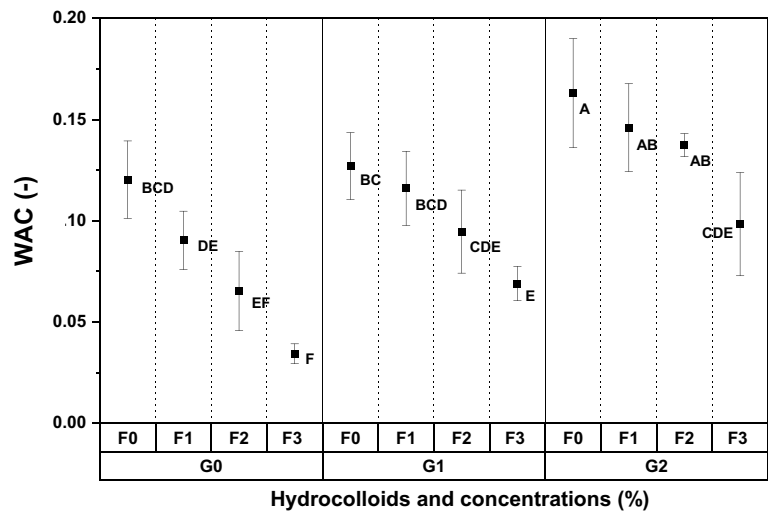
the parallel direction compared to the perpendicular direction (Figs. 5A). This finding suggests that the products exhibited anisotropic behavior (Fig. 5B). Nonetheless, the difference between the parallel and perpendicular values was negligible and not particularly noticeable. The products exhibited short and thin fibrillar filaments at a micro-scale (Tables 4 and 5), which was also observed at a macro-scale (Tables 2 and 3). Both the parallel and the perpendicular tensile stress values of these products were significantly ($p \leq 0.05$) lower than those of F0-G0, F1-G0, F2-G0, and F3-G0.

In a previous investigation conducted by Taghian Dinani et al. [22], the impact of various hydrocolloids on PPI + WG blends subjected to 120 °C for 15 min was explored. The findings revealed that among the hydrocolloids tested, low acyl gellan gum demonstrated the most substantial enhancement in tensile stress values in both parallel and perpendicular directions when compared to the other hydrocolloids and the control. The authors postulated that this rise in tensile strength might be attributed to the extensive networks formed by low acyl gellan gum during processing, resulting in increased viscosity and enhanced resistance against flow. The variation in the findings could be attributed to the distinct raw materials employed in the current study, specifically SPI as opposed to the PPI + WG blend utilized by [22]. It is plausible that low acyl gellan gum exhibits a stronger affinity for WG protein or PPI protein, resulting in more stabilizing interactions and, consequently, elevated tensile strength, fiber formation, and stabilization.

Technological parameter of water absorption capacity

The WAC is a critical quality attribute in plant-based meat analogs as it indicates the level of juiciness and evaluates the ability of proteins to hold water and form a protein gel network. Figure 6 illustrates that as the concentration of insoluble soy fiber increases, the WAC decreases significantly compared to the control product. In more detail, it illustrates that as the concentration of insoluble soy fiber increases (F1-G0, F2-G0, and F3-G0), the WAC decreases significantly compared to the control product ($p \leq 0.05$). The decrease in WAC for these products can be attributed to the effect of thermomechanical processing, which could be due to the formation of large-molecular-weight aggregates resulting from cross-linking. Since products F1-G0, F2-G0, and F3-G0 have a more fibrous structure than other products, the amount of large-molecular-weight aggregates is also higher. This increase in aggregate amount may be responsible for the reduction in WAC when the fiber concentration of the products is increased. This phenomenon is apparent at both macro- (Tables 2 and 3) and micro-scales (Tables 4 and 5).

Fig. 6 Water holding capacity (WAC) (–) of products with and without the addition of insoluble soy fiber (F) and/or low acyl gellan gum (G). In this figure, data are represented as mean \pm SD and different English letters show statistically significant difference of data ($p \leq 0.05$)



Insoluble soy fiber is mainly made up of hydrocolloids like cellulose that are not soluble in water. As a result, a higher percentage of insoluble compounds in the formula led to a decrease in WAC. Additionally, the increase in the concentration of insoluble soy fiber reduced the concentration of SPI from 39 to 36 wt.% which, in turn, reduced the ability of the protein to absorb water. Interestingly, the void fractions in products F1-G0, F2-G0, and F3-G0 did not contribute to an increase in WAC. Despite the presence of voids, these products still exhibited a lower WAC because of the reasons mentioned above.

The study's findings on WAC showed that products with higher concentrations of low acyl gellan gum, especially those containing 2 wt.% low acyl gellan gum (F0-G2), had a significant increase ($p \leq 0.05$) in WAC. This could be attributed to low acyl gellan gum's ability to act as a water-soluble hydrocolloid, which can stabilize and retain large amounts of water. Furthermore, the increase in WAC was also observed in gluten-free pasta made of maize and oat flours with the addition of 2 wt.% low acyl gellan gum [15]. In their research, low acyl gellan gum significantly increased ($p \leq 0.05$) the WAC capacity to $155 \pm 10\%$, compared to the control group of maize and oat flour, which absorbed $132 \pm 16\%$ water.

On the other hand, it was also noted that the introduction of insoluble soy fiber to the formulations containing low acyl gellan gum (F1-G1, F2-G1, F3-G1, F1-G2, F2-G2, and F3-G2) resulted in a decrease in WAC (as depicted in Fig. 6). This reduction could be explained by the presence of insoluble components in the formulation, such as cellulose, which is incapable of absorbing water. The downward trend of WAC was consistently observed each time insoluble soy fiber was incorporated into the formulation, indicating the adverse impact of its addition on the products' WAC.

Conclusions

This research studied the impact of insoluble soy fiber (0–3%), low acyl gellan gum (0–2%), and their combination on a blend of soy protein isolate, water, and CaCl_2 , which underwent thermomechanical processing using the HTSC. The inclusion of insoluble soy fiber in plant-based meat analogs resulted in significant effects observed at both macroscopic and microscopic levels. Products containing insoluble soy fiber but without low acyl gellan gum exhibited dense, gel-like properties. The fibers within these products elongated in the shear direction and displayed orientation dependency, as validated by CLSM and SEM images. The presence of a substantial air fraction played a pivotal role in the formation of fibers and the anisotropy of these products. The tensile strength of the insoluble soy fiber-containing products increased notably when measuring parallel to the shear flow direction as opposed to perpendicular to it, indicating the presence of anisotropy. This effect was visually confirmed by the presence of visible fibers orientated in the shear direction. Additionally, the insoluble soy fiber-containing products exhibited the lowest values of $\tan \delta$ pointing to elasticity. Products containing low acyl gellan gum, either alone or in combination with insoluble soy fiber, resulted in the formation of short, brittle, fibrillar structures upon bending. These fibrillar components were elongated in the shear direction, indicating anisotropy, which corresponded with macroscopic and microscopic observations. For instance, CLSM images revealed a somewhat oriented protein phase in the products in the direction of shear flow. Furthermore, the addition of low acyl gellan gum increased the water absorption capacity of the products, likely due to the formation of smaller aggregates or the water-absorbing

properties of low acyl gellan gum. These findings hold potential implications for the development of new food products using SPI without the inclusion of gluten through HTSC processing.

Appendix A: supplementary data

Table S1 (see Table 7)

Figures S1, S2, S3 (see Figs. 7, 8, 9)

Table 7 3D X-ray microtomography (XRT) images representing the solid part of plant-based meat alternatives with and without the addition of insoluble soy fiber (F) and or low acyl gellan gum (G)

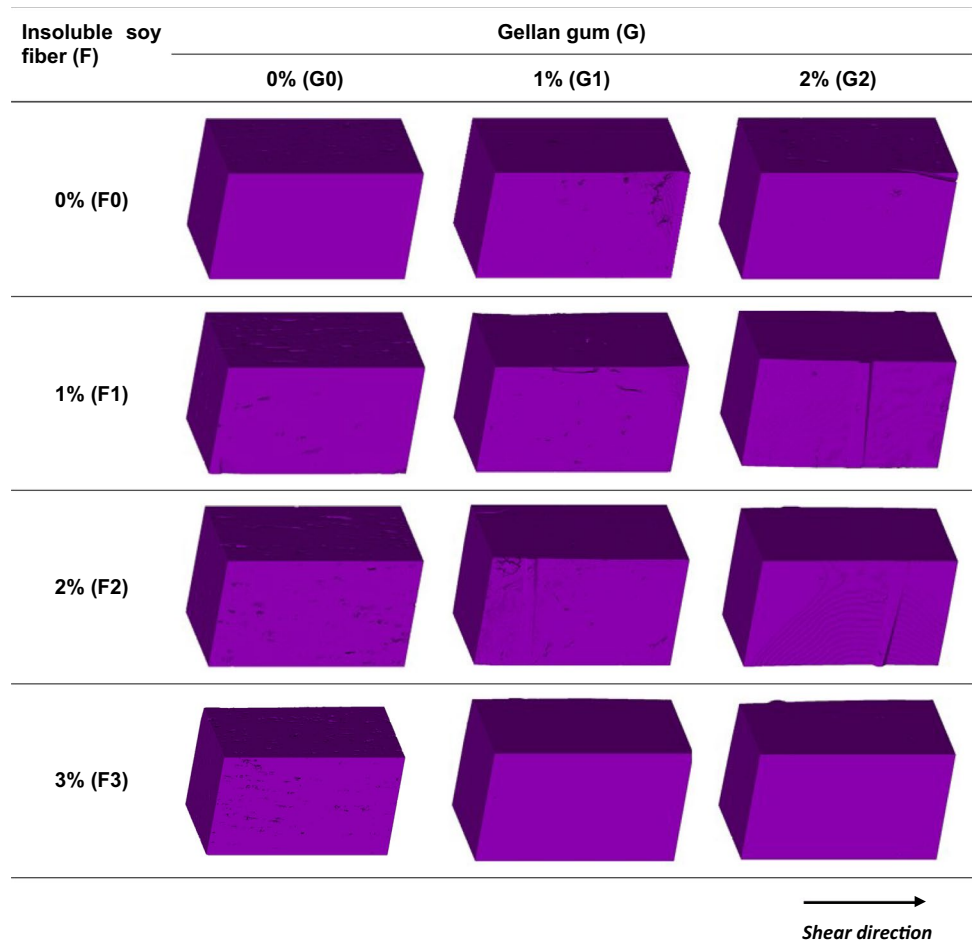


Fig. 7 Average bubble volume (mm^3) of HTSC processed samples obtained from data analysis of 3D X-ray microtomography (XRT) images representing air inclusion in HTSC plant-based meat alternatives for all products with and without the addition of insoluble soy fiber (F) and/or low acyl gellan gum (G). In this figure, data are represented as mean \pm SD and different English letters show statistically significant difference of data ($p \leq 0.05$)

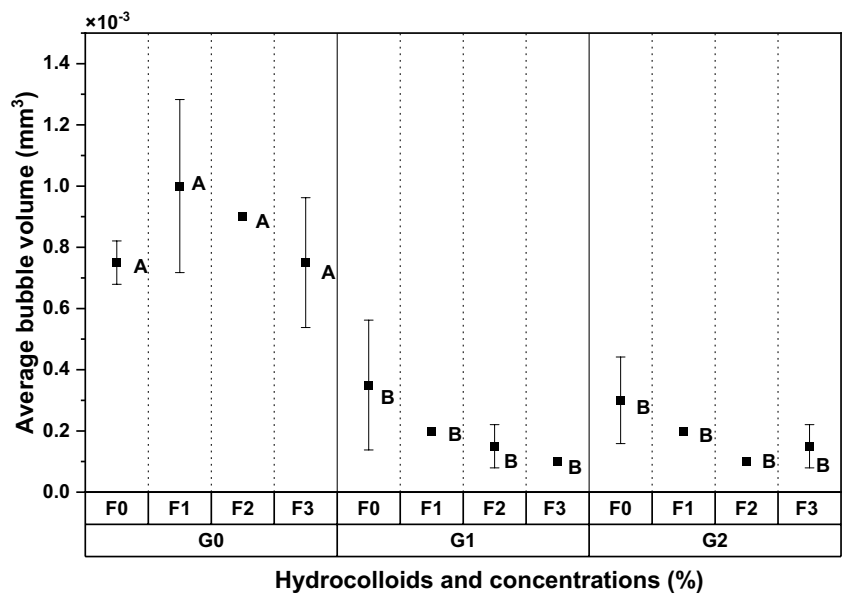


Fig. 8 The storage (G') and loss modulus (G'') for formulations with and without the addition of insoluble soy fiber (F) and/ low acyl gellan gum (G) after **A** 15 min heating at 120 °C, 80% strain, and frequency 10 Hz and **B** 7.5 min cooling at a constant cooling rate of 5 °C/min C, 80% strain, and frequency 10 Hz in the CCR. In this figure, data are represented as mean \pm SD and different English letters show statistically significant difference of data ($p \leq 0.05$)

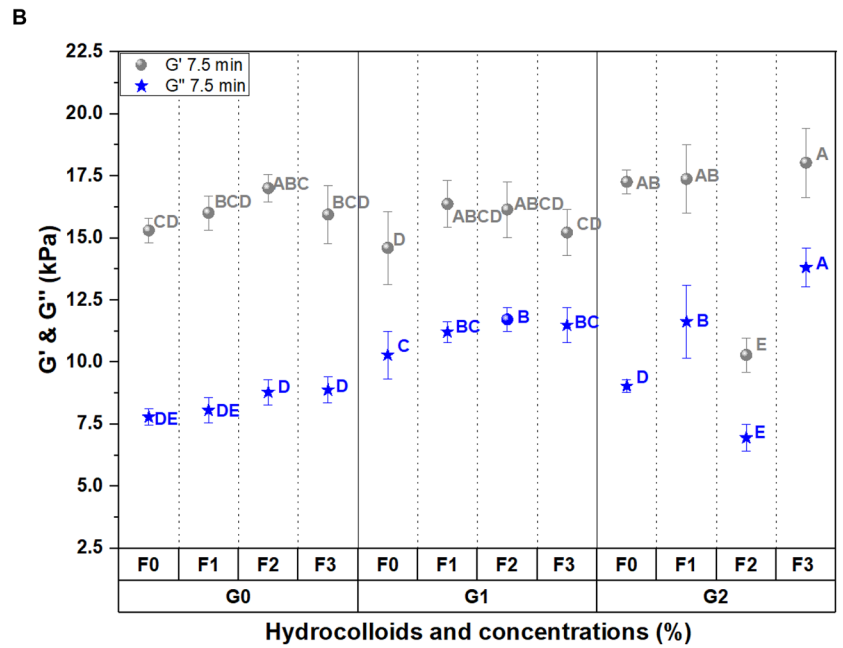
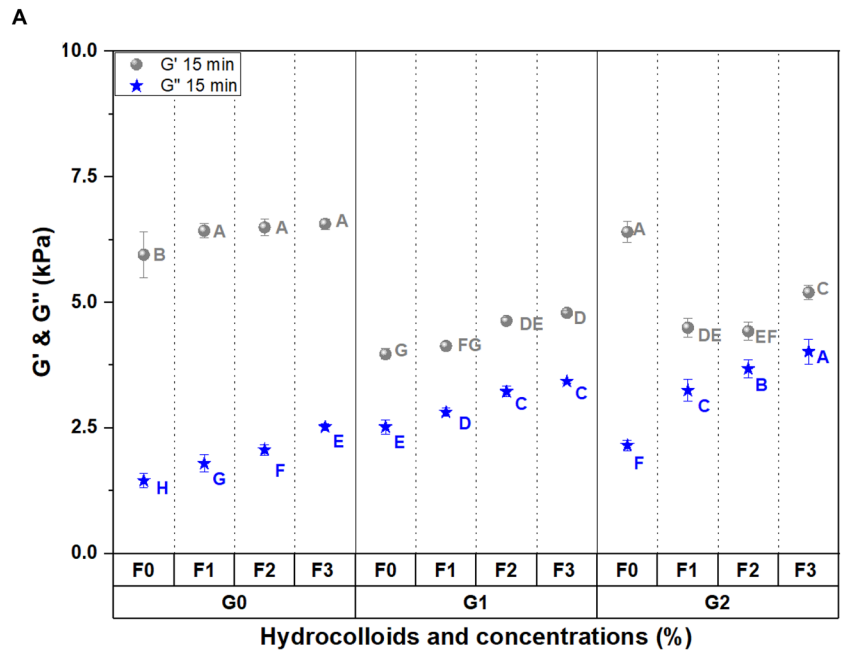
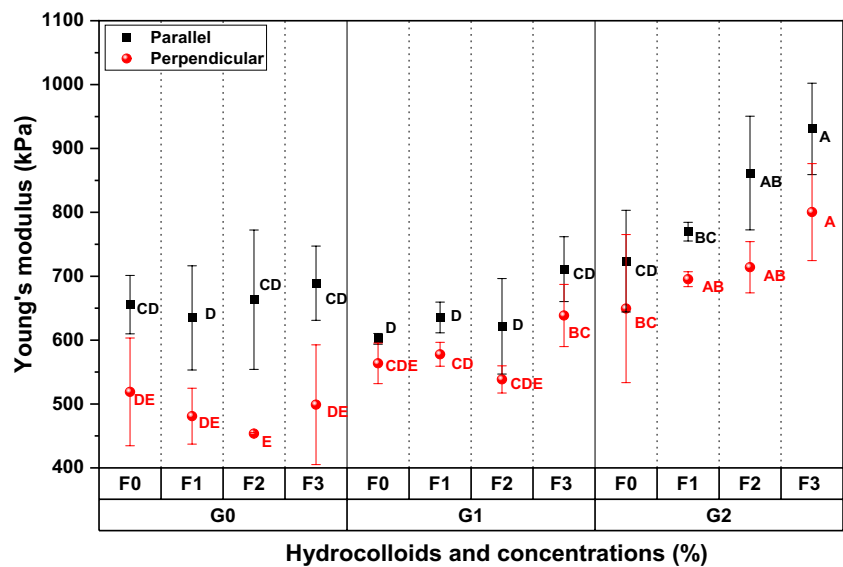


Fig. 9 Young's modulus (kPa) for products with and without the addition of insoluble soy fiber (F) and/or low acyl gellan gum (G) sheared for 15 min, 30 rpm at 120°C deformed in parallel (■) and perpendicular (●) direction. In this figure, data are represented as mean \pm SD and different English letters show statistically significant difference of data ($p \leq 0.05$)



Acknowledgements This research is part of the project PlantPromise and co-financed by Top Consortium for Knowledge and Innovation Agri & Food by the Dutch Ministry of Economic Affairs as well as the United Soybean Board and Foundation for Food and Agriculture Research. The authors would like to thank Jarno Gieteling, Jos Sewalt, Maurice Strubel, Maaik Nieuwland, Jelmer Vroom, Wouter de Groot, and Martin de Wit for their technical support.

Funding Plant Promise, United Soybean Board.

Declarations

Conflict of interest All authors declare that there is no conflict of interest.

Compliance with ethics requirements This study does not contain any studies with human participation or animals performed by any of the authors.

Open Access This article is licensed under a Creative Commons Attribution 4.0 International License, which permits use, sharing, adaptation, distribution and reproduction in any medium or format, as long as you give appropriate credit to the original author(s) and the source, provide a link to the Creative Commons licence, and indicate if changes were made. The images or other third party material in this article are included in the article's Creative Commons licence, unless indicated otherwise in a credit line to the material. If material is not included in the article's Creative Commons licence and your intended use is not permitted by statutory regulation or exceeds the permitted use, you will need to obtain permission directly from the copyright holder. To view a copy of this licence, visit <http://creativecommons.org/licenses/by/4.0/>.

References

- Beniwal AS, Singh J, Kaur L, Hardacre A, Singh H (2021) Meat analogs: protein restructuring during thermomechanical processing. *Compr Rev Food Sci Food Saf* 20(2):1221–1249. <https://doi.org/10.1111/1541-4337.12721>
- Cornet SHV, Snel SJE, Schreuders FKG, van der Sman RGM, Beyrer M, van der Goot AJ (2022) Thermo-mechanical processing of plant proteins using shear cell and high-moisture extrusion cooking. *Crit Rev Food Sci Nutr* 62(12):3264–3280. <https://doi.org/10.1080/10408398.2020.1864618>
- Dekkers BL, Emin MA, Boom RM, van der Goot AJ (2018) The phase properties of soy protein and wheat gluten in a blend for fibrous structure formation. *Food Hydrocoll* 79:273–281. <https://doi.org/10.1016/j.foodhyd.2017.12.033>
- Dekkers BL, Hamoen R, Boom RM, van der Goot AJ (2018) Understanding fiber formation in a concentrated soy protein isolate - pectin blend. *J Food Eng* 222:84–92. <https://doi.org/10.1016/J.JFOODENG.2017.11.014>
- Dekkers BL, Nikiforidis CV, van der Goot AJ (2016) Shear-induced fibrous structure formation from a pectin/SPI blend. *Innov Food Sci Emerg Technol* 36:193–200. <https://doi.org/10.1016/J.IFSET.2016.07.003>
- Dinani ST, Broekema NL, Boom RM, van der Goot AJ (2023) When and how should low acyl gellan gum be added to the protein blends to improve meat analogue texture? *J Food Meas Charact.* <https://doi.org/10.1007/s11694-023-02137-7>
- Erdman JW, Badger TM, Lampe JW, Setchell KDR, Messina M (2004) Not all soy products are created equal: caution needed in interpretation of research results. *J Nutr* 134(5):S1229–S1233. <https://doi.org/10.1093/JN/134.5.1229S>
- Grabowska KJ, Tekidou S, Boom RM, van der Goot AJ (2014) Shear structuring as a new method to make anisotropic structures from soy-gluten blends. *Food Res Int* 64:743–751. <https://doi.org/10.1016/j.foodres.2014.08.010>
- Grabowska KJ, Zhu S, Dekkers BL, de Ruijter NCA, Gieteling J, van der Goot AJ (2016) Shear-induced structuring as a tool to make anisotropic materials using soy protein concentrate. *J Food Eng* 188:77–86. <https://doi.org/10.1016/j.jfoodeng.2016.05.010>
- Guo M (2009) Soy food products and their health benefits. In: Guo M (ed) *Functional foods*. Woodhead Publishing, pp 237–277. <https://doi.org/10.1533/9781845696078.237>
- Hartmann C, Siegrist M (2020) Our daily meat: justification, moral evaluation and willingness to substitute. *Food Qual Preference* 80:103799. <https://doi.org/10.1016/j.foodqual.2019.103799>
- Hoek AC, Luning PA, Weijzen P, Engels W, Kok FJ, de Graaf C (2011) Replacement of meat by meat substitutes. A survey on person- and product-related factors in consumer acceptance. *Appetite* 56(3):662–673. <https://doi.org/10.1016/j.appet.2011.02.001>

13. Jia W, Curubeto N, Rodríguez-Alonso E, Keppeler JK, van der Goot AJ (2021) Rapeseed protein concentrate as a potential ingredient for meat analogues. *Innov Food Sci Emerg Technol* 72:102758. <https://doi.org/10.1016/J.IFSET.2021.102758>
14. Morris ER, Nishinari K, Rinaudo M (2012) Gelation of gellan – a review. *Food Hydrocoll* 28(2):373–411. <https://doi.org/10.1016/J.FOODHYD.2012.01.004>
15. Padalino L, Mastromatteo M, De Vita P, Maria Ficco DB, Del Nobile MA (2013) Effects of hydrocolloids on chemical properties and cooking quality of gluten-free spaghetti. *Int J Food Sci Technol* 48(5):972–983. <https://doi.org/10.1111/ijfs.12049>
16. Schlangen M, Ribberink MA, Taghian Dinani S, Sagis LMC, van der Goot AJ (2023) Mechanical and rheological effects of transglutaminase treatment on dense plant protein blends. *Food Hydrocoll* 136:108261. <https://doi.org/10.1016/j.foodhyd.2022.108261>
17. Schreuders FKG, Bodnár I, Erni P, Boom RM, der Goot AJ, van. (2020) Water redistribution determined by time domain NMR explains rheological properties of dense fibrous protein blends at high temperature. *Food Hydrocoll*. <https://doi.org/10.1016/j.foodhyd.2019.105562>
18. Schreuders FKG, Dekkers BL, Bodnár I, Erni P, Boom RM, van der Goot AJ (2019) Comparing structuring potential of pea and soy protein with gluten for meat analogue preparation. *J Food Eng* 261:32–39. <https://doi.org/10.1016/j.jfoodeng.2019.04.022>
19. Schreuders FKG, Schlangen M, Bodnár I, Erni P, Boom RM, van der Goot AJ (2022) Structure formation and non-linear rheology of blends of plant proteins with pectin and cellulose. *Food Hydrocolloids* 124:107327. <https://doi.org/10.1016/j.foodhyd.2021.107327>
20. Statista (2022) Meat - Worldwide | Statista Market Forecast. <https://www.statista.com/outlook/cmo/food/meat/worldwide>
21. Taghian Dinani S, Allaire N, Boom R, van der Goot AJ (2023) Influence of processing temperature on quality attributes of meat analogues fortified with l-cysteine. *Food Hydrocoll* 137:108422. <https://doi.org/10.1016/j.foodhyd.2022.108422>
22. Taghian Dinani S, Broekema NL, Boom R, van der Goot AJ (2023) Investigation potential of hydrocolloids in meat analogue preparation. *Food Hydrocoll* 135:108199. <https://doi.org/10.1016/j.foodhyd.2022.108199>
23. Taghian Dinani S, Charles Carrillo MF, Boom R, van der Goot AJ (2023) Quality improvement of plant-based meat alternatives by addition of iota carrageenan to pea protein–wheat gluten blend. *Eur Food Res Technol*. <https://doi.org/10.1007/s00217-023-04244-7>
24. Taghian Dinani S, van der Harst JP, Boom R, van der Goot AJ (2023) Effect of L-cysteine and L-ascorbic acid addition on properties of meat analogues. *Food Hydrocoll*. <https://doi.org/10.1016/j.foodhyd.2022.108059>
25. Taghian Dinani S, Zhang Y, Vardhanabhuti B, van der Goot AJ (2023) Enhancing textural properties in plant-based meat alternatives: the impact of hydrocolloids and salts on soy protein-based products. *Curr Res Food Sci*. <https://doi.org/10.1016/j.crfs.2023.100571>
26. Theethira TG, Dennis M (2015) Celiac disease and the gluten-free diet: consequences and recommendations for improvement. *Dig Dis* 33(2):175–182. <https://doi.org/10.1159/000369504>
27. United Nations (2022) Population. <https://www.un.org/en/global-issues/population>
28. Wang Z, Tian B, Boom R, van der Goot AJ (2019) Air bubbles in calcium caseinate fibrous material enhances anisotropy. *Food Hydrocoll* 87:497–505. <https://doi.org/10.1016/j.foodhyd.2018.08.037>

Publisher's Note Springer Nature remains neutral with regard to jurisdictional claims in published maps and institutional affiliations.